Chapter 5 – Ideal Magnetohydrodynamics Stability

5.1 Overview

In this chapter, we consider ideal stability of various MHD modes ranging from low mode number (vertical modes, external kink modes) to infinite n (ballooning modes, Mercier modes). We will discuss general MHD stability properties of compact QAS with finite plasma current and various stabilization mechanisms. We will present details of stability results for the NCSX reference configuration. Much of the results have already been published [1,2,3,4,5,6].

In our design study, we have used the most advanced 3D MHD stability codes available, such as Terpsichore-VVBAL [7] and COBRA [8,9] for infinite-n ballooning modes, Terpsichore [10] and CAS3D [11] for global moderate-n external kink modes. These codes are essential for self-consistent stability prediction of beta limits in stellarators. Extensive work has been done to benchmark these stability codes.

The NCSX configuration is closely related to advanced tokamaks with reversed shear. In fact, the initial design of NCSX started from an optimized reversed shear tokamak (ARIES design) by adding appropriate 3D shaping which generates external rotational transform while maintaining quasisymmetry. Due to quasi-axisymmetry, the bootstrap current in NCSX is similar to that in an equivalent tokamak. Therefore, like in a tokamak, both the plasma current and pressure drive MHD instabilities in the NCSX [3]. However, the MHD stability in the NCSX differs significantly from an advanced tokamak due to stabilizing influences of 3D shaping. As a result, the external kink modes are much more stable as compared to an advanced tokamak.

3D shaping of a QAS can influence the MHD stability in several ways as compared to an advanced tokamak. 3D shaping generates external rotational transform. This is stabilizing for both vertical and external kink modes because a smaller plasma current is present to drive instability at fixed edge iota. 3D shaping also modifies iota profile that affects MHD stability strongly. 3D shaping also strongly affects local magnetic shear and curvature that are important to MHD stability. Our optimization experience shows that 3D shaping can be used effectively to enhance MHD stability of a compact QAS. The NCSX reference configuration (LI383) is a product of such an optimization via 3D shaping.

This chapter is organized as follows. Section 5.2 describes the main stability codes used in this work and their benchmarks. Section5.3 discusses general stability properties of compact QAS. Section 5.4 presents detailed stability analysis of the NCSX configurations for external kink modes and vertical modes as well as ballooning modes. Section 5.5 discusses the effects of wall on external kink stability. Section 5.6 discusses the Toroidal Alfvén Eigenmodes in the NCSX. Finally, a summary is given in Section 5.7 .

5.2 Numerical Codes and Benchmarks

The NCSX design uses the most advanced codes for its stability calculations. Among them, the ballooning stability is calculated using two codes: Terpsichore-VVBAL [7] and Cobra [8,9]. The global kink and vertical mode stability is calculated using both Terpsichore [10] and CAS3D [11]. All these stability codes are based on numerical equilibria as computed by the 3D code VMEC [12].

5.2.1 Equilibrium code VMEC

The 3D equilibrium code VMEC [12] solves for 3D equilibria by minimizing plasma potential energy. A key assumption of the code is that the flux surfaces are closed. As a result, magnetic islands are not allowed. Our stability calculations are also based on this assumption. We expect that the VMEC solutions are good approximations of real equilibria when magnetic islands are small and the stability results should be reliable especially for global kink modes that are largely determined by global equilibrium profiles.

5.2.2 Ballooning codes Terpsichore and Cobra

The Terpsichore-VVBAL ballooning code [7] solves the standard ballooning mode equation in Boozer coordinates [13]:

$$\rho\gamma^2 \left(\mathbf{k}_\perp^2/B^2\right) \Phi - \mathbf{B} \bullet \nabla\left(\mathbf{k}_\perp^2/B^2\right)\mathbf{B} \bullet \nabla\Phi - p'/B^2 \left(\mathbf{k}_\perp \times \mathbf{B}\right) \bullet \kappa\Phi = 0 \quad (5\text{-}1)$$

where $\mathbf{k}_\perp = \nabla\phi - q(\psi)\nabla\theta - q'(\theta - \theta_k)\nabla\psi$ with θ_k being the radial wave number. In Eq. (5-1), the first term is from the kinetic energy, the second term corresponds to the field line bending energy, and the last term corresponds to the destabilizing drive due to bad curvature and pressure gradient. A major part of the code is mapping from VMEC coordinates to straight field line Boozer coordinates. The ballooning equation is solved using a shooting method and the eigenvalue is a function of s, θ_k, and $\alpha = \phi - q\theta$ where α is the field line variable. Note that unlike in tokamaks, the local ballooning eigenvalues also depend on α in stellarators due to 3D geometry. The most unstable eigenvalue in the space of (s,θ_k,α) determines the beta limit. Instead of solving for eigenvalue ω^2 in Eq. (5-1), the following marginal equation is solved with λ as an eigenvalue:

$$\mathbf{B} \bullet \nabla \left(\mathbf{k}_\perp^2/B^2\right) \mathbf{B} \bullet \nabla\Phi + (1 - \lambda) \left(p' / B^2\right) \left(\mathbf{k}_\perp \times \mathbf{B}\right) \bullet \kappa\Phi = 0 \quad (5\text{-}2)$$

where $(1-\lambda)$ is a multiplier to the destabilizing curvature term. Note that $\lambda > 0$ for instability. This method is advantageous over solving for ω^2 because the eigenvalue λ is well defined for both unstable and stable cases. In contrast, the eigenvalue γ^2 is a continuous spectrum for stable cases in Eq. (5-1) and is not well defined numerically.

The ballooning code COBRA [8] solves the ideal ballooning equation for the growth rate using finite element method. Eq. (5-1) then becomes a matrix equation. The computation can be done in an extremely efficient and accurate way by taking advantage of the Stürm-Lioville character of the ballooning equation. This property allows to estimate the growth rate to 4th order on the mesh step size along the magnetic field line by variationally refining a previous 2nd order estimated obtained from a standard matrix method. Fast evaluation is made possible by coupling this evaluation process to a Richardson's extrapolation scheme, that will extrapolate to zero mesh step size from a few previous evaluations of the growth rates computed on very coarse (and therefore easy to evaluate) meshes. Important speed enhancements (of hundreds of times) relative to standard codes can be achieved in this way [8]. Recently, a VMEC-based version of COBRA [9] has been developed as a result of several convergence problems appearing on the Boozer-coordinate-based COBRA (namely, the growth rate would sometimes change when the number of Boozer modes included in the equilibrium mapping from the VMEC equilibrium solution, turning unstable previously ascertained stable cases). In this latest version, the magnetic field line must be numerically followed at the same time that the ballooning equation is solved in a way that does not interfere with the Richardson's scheme. This has been achieved by locating the magnetic field line at each mesh point via a Newton-Raphson scheme [9].

We have used both Terpsichore-VVBAL and Cobra in our configuration design. The Terpsichore ballooning code was exclusively used in the past until Cobra became available recently. Since Cobra is a much faster code, we have used it extensively in the search of plasma configurations that are stable to ballooning modes at high beta.

To validate these two ballooning codes, we have made benchmark comparisons between them. The first case of comparison is a QHS configuration that is unstable to ballooning modes at β as low as 2%. At this beta, the configuration is Mercier stable so that the ballooning stability results are not sensitive to the length of integration. Figure 5-1 on the left shows the comparison of the eigenvalues as a function of the normalized toroidal flux (Note that the normalization for eigenvalues of the two codes are different). Good agreement of the unstable region is evident in the figure. It should be noted here that The definitions of the eigenvalue are different in the two codes so that the absolute size of the eigenvalue does not agree. We have also compared the results of the two codes for the QAS configuration C82, which was the reference configuration for NCSX a year ago. A comparison of a 4% beta case is shown in Figure 5-1 on the right. Again, the region of ballooning instability matches well in two codes. The fluctuation in eigenvalue in the stable region calculated by Terpsichore is due to the resonances and the broadening of the eigenfunction which requires even larger boxes of integration to obtain better solutions. The important conclusion, however, is that the unstable region agrees well.

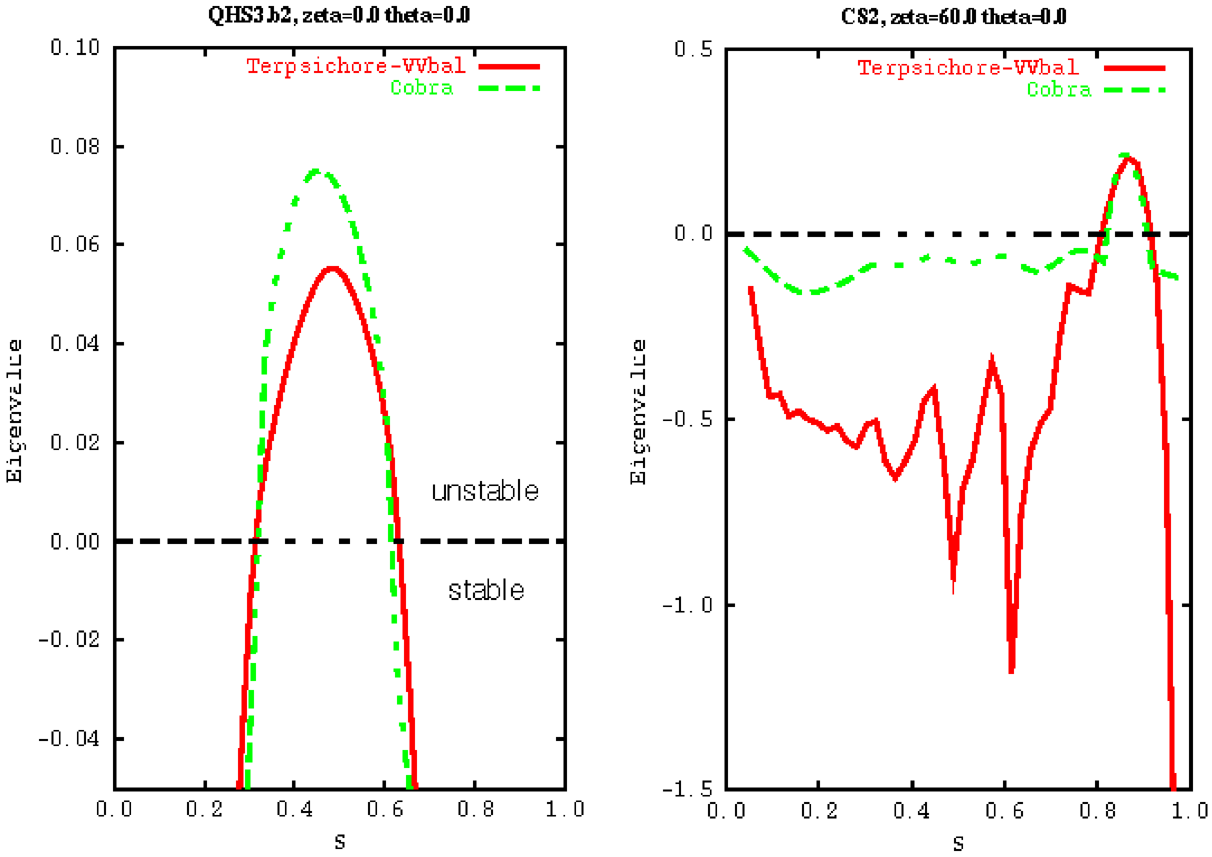

Figure 5-1. Ballooning eigenvalues obtained with Terpsichore (red) and COBRA (green) as function of normalized toroidal flux S for a QHS stellarator (left) and a QAS stellarator (right)

5.2.3 Global 3D codes Terpsichore and CAS3D

The three dimensional ideal MHD stability code Terpsichore [10] is used to calculate the stability of global MHD modes. The code determines the eigenvalues of the ideal MHD equations by minimizing the plasma potential energy as defined in the energy principle [14]:

$$\omega^2\, \delta W_k = \delta W_p + \delta W_{vac} \tag{5-3}$$

where $-\omega^2\, \delta W_k$ is the kinetic energy, δW_{vac} is the magnetic energy in the vacuum region between plasma and conducting wall, and δW_p is the plasma potential energy written as

$$\delta W_p = 1/2 \int d^3x\, \{\, \delta \mathbf{B}_\perp{}^2 + [\delta \mathbf{B}_{||} - \mathbf{B}\, (\xi \bullet \nabla\, p/B^2)]^2$$

$$+ \Gamma(\nabla \bullet \xi)^2 + \mathbf{j}_{||} \bullet \xi \times \delta \mathbf{B} - 2\, \xi \bullet \nabla p\, \xi \bullet \kappa\} \tag{5-4}$$

where $\delta\mathbf{B}$ is the perturbed magnetic field, ξ is the plasma displacement vector, Γ is the coefficient of specific heat, $\mathbf{j}_{||}$ is the parallel equilibrium current along the field line, and κ is the magnetic curvature. The displacement vector is written as

$$\xi = \sqrt{g}\, \xi^s\, \nabla\theta \times \nabla\phi + \eta(\mathbf{B} \times \nabla s/B^2) \tag{5-5}$$

where s, θ, and ϕ are radial, poloidal and toroidal variables in Boozer coordinates. Note that $\delta\mathbf{B} = \nabla\times(\xi\times\mathbf{B})$ in ideal MHD. In Eq. (5-4), the first and second terms in the integrand are the stabilizing field line bending energy and the magnetic field compression energy respectively, the third term is the fluid compression energy, the fourth term is destabilizing due to parallel current and is responsible for kink instabilities. Lastly, the fifth term is usually destabilizing due to unfavorable curvature and pressure gradient.

It should be pointed out that for most of our results an artificial kinetic energy is used for simplicity. This artificial kinetic energy is given by $\delta W_k = (1/2)\int d^3x\, [(\xi^s)^2 + (\eta)^2]$. As a result, the plasma displacement is incompressible since the parallel component only appears in the fluid compression term. Although the calculated eigenvalue does not correspond to the physical growth rate, the marginal stability boundary remains the same. Recently, a new version of Terpsichore becomes available which uses physical kinetic energy and can calculate physical growth rate at $\Gamma = 0$.

The Terpsichore code uses Fourier decomposition in poloidal and toroidal angles and a finite element method for radial discretization The radial and surface component of the plasma displacement vector are represented by sums of Fourier series:

$$\xi^s(s,\theta,\phi) = \sum \xi_l(s)\sin(m_l\theta - n_l\phi + \Delta)$$

$$\eta(s,\theta,\phi) = \sum \eta_l(s)\cos(m_l\theta - n_l\phi + \Delta) \qquad (5\text{-}6)$$

where Δ is a phase factor and the subscript l is an index for each pair of poloidal and toroidal mode numbers (m,n). The radial dependence is represented by piece-wise linear elements for ξ_l and piece-wise constant elements for η. After minimization of the plasma potential energy, the problem reduces to an eigenvalue problem of a linear matrix equation. The eigenvalue system is solved by an inverse iteration method that can converge towards the most unstable eigenvalue. An accurate eigenvalue requires sufficient radial grid points and poloidal/toroidal modes for both the equilibrium and the perturbation.

The Terpsichore code uses a pseudo-plasma method for evaluation of the magnetic perturbation in the vacuum. In this method, the perturbed magnetic field in vacuum is written the same way as in plasma: $\delta B = \nabla\times(\xi\times\mathbf{B}_v)$, but here B_v is a shearless pseudo-magnetic field. It can be shown that this representation is general as long as B_v is shearless. In this way, the vacuum region can be treated as a pressureless and currentless plasma and can be solved in the same way as in plasma.

The CAS3D [11] code is similar to Terpsichore in many aspects. It uses the same representations of the equilibrium and the perturbation as in Terpsichore and solves the same type of matrix equation for unstable eigenvalue. However, it differs significantly from Terpsichore in the treatment of vacuum. The CAS3D uses a Green function method in calculating the vacuum magnetic energy. Thus it can compute free boundary stability without a conducting wall. In contrast, a conducting wall is necessary present in Terpsichore model because it uses a finite grid for the vacuum. In practice, the conducting wall can be put far away so that the effects of the wall is minimal on the stability of external kink modes and the associated beta limits.

The Terpsichore code has been used for most of MHD calculations in the NCSX project for the sake of code speed. The CAS3D is used to benchmark the Terpsichore results and for some of the stability analysis.

The MHD calculations in stellarators differ from axisymmetric tokamaks in several ways. A key difference lies in Fourier mode selection for the perturbation. Unlike in tokamaks, different toroidal modes are coupled together due to 3D geometry. For stellarators with field period N_p, Fourier harmonics with toroidal mode number n are coupled to $n+kN_p$, where k is an arbitrary integer. There are $N_p/2+1$ families of modes for even N_p and $(N_p-1)/2+1$ families for odd N_p. For example, there are two families (N = 0, N = 1) for both $N_p = 2$ and $N_p = 3$ and there are three families (N = 0, N = 1 and N = 2) for $N_p = 4$. Within one family of modes, there are infinite number of eigenmodes with different mode spectra. Typically, the external kink modes have low toroidal mode numbers for the dominating harmonics. The vertical mode in stellarators belongs to the N = 0 family which preserves the stellarator periodicity. However, an eigenmode of the N = 0 family can have characteristics of a kink or ballooning mode when the dominating toroidal mode number is not zero.

A subtle issue of 3D stability calculations is the phase dependence. In tokamaks, the stability is independent of the phase due to axisymmetry. This is not so for the N = 0 family in stellarators. The stability also depends on the phase for the N = $N_p/2$ family when N_p is even. Assuming stellarator symmetry for the underlying equilibrium, only two values of the phase, $\Delta = 0$ (sin phase) and $\Delta = \pi/2$ (cos phase), are meaningful because the modes with sin phase are decoupled from the modes with cos phase. The phase should be zero for the N = 0 vertical mode.

The Terpsichore code has been benchmarked extensively. Earlier it was shown [15] that the Terpsichore's stability results agree well with 2D stability codes for growth rates of fixed boundary MHD modes in 2D analytic Solov'ev equilibria. In the present work, we have benchmarked Terpsichore against the 2D stability code PEST[16] and the 3D code CAS3D [11] for external kink modes for an optimized reversed shear tokamak equilibrium from the ARIES studies [17]. The calculated beta limit of the n = 1 external kink mode using Terpsichore is 2.34%, which agrees well with the PEST result of 2.4% and the CAS3D result of 2.3% [20]. We have also benchmarked the code for the n = 0 vertical mode in a large aspect ratio tokamak.

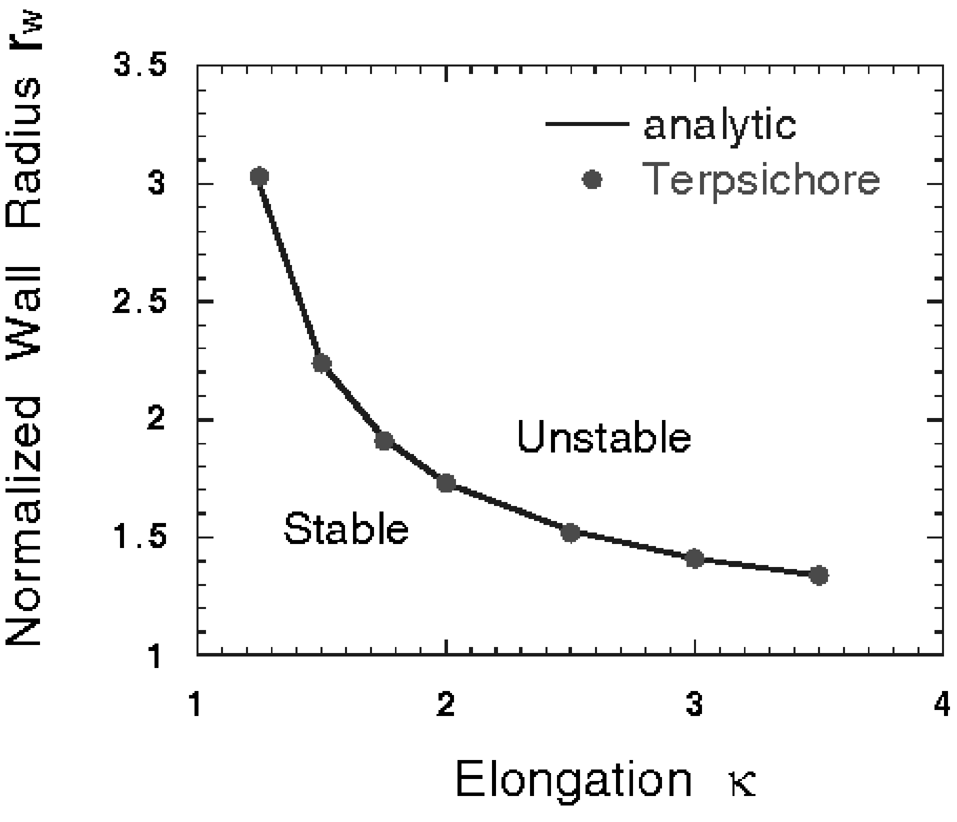

Figure 5-2. The critical normalized wall radius versus elongation for a elliptical plasma

Figure 5-2 plots the critical wall radius as function of ellipticity for the stability of the n = 0 vertical mode in an elliptical plasma with constant current density profile and zero beta. The

Terpsichore results (shown in dots) agree well with the analytic stability criterion [18] (solid line) give by

$$r_w = \sqrt{\frac{\kappa+1}{\kappa-1}} \tag{5-7}$$

where the normalized wall radius is defined by $r_w = (a' + b')/(a+b)$ with a and b (a' and b') being the radius of the elliptical plasma (a confoncal wall) along the horizontal and vertical direction respectively. Here, $\kappa = b/a$. Most recently, we have compared stability results of Terpsichore with those of CAS3D for a real 3D stellarator equilibrium with finite beta and current [19]. Figure 5-3 shows the growth rates of the N = 1 external kink mode obtained by Terpsichore and CAS3D as function of plasma beta for the previous NCSX configuration C82. The results are obtained with 108 pairs of (m,n) for the kink mode and are converged in radial grid points and equilibrium Fourier modes. The CAS3D results are obtained without a conducting wall. The Terpsichore results are obtained with a conducting wall 2.5a away from the plasma edge so that the effects of wall on the beta limit should be negligible. We can then conclude that the Terpsichore's stability thresholds agree fairly well with those of CAS3D, at least for C82.

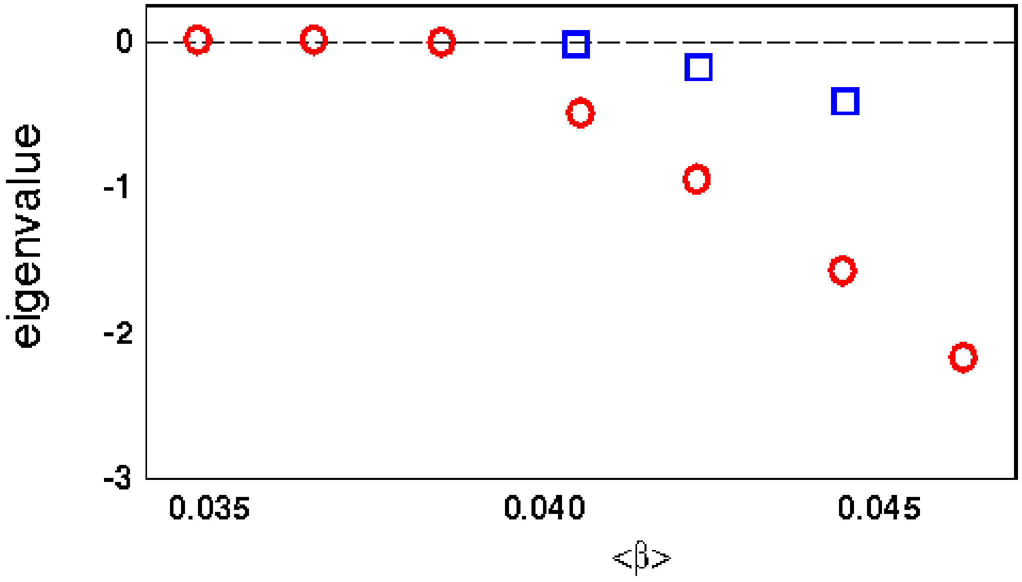

Figure 5-3. The N = 1 external kink eigenvalues as function of plasma beta obtained with CAS3D (open circles) and Terpsichore (open squares)

5.3 Kink and Vertical Mode Stability

Here we present general features of kink and vertical stability in a current-carrying finite beta compact QAS [4,6] and specific results for NCSX reference configuration. As described in the previous sections, the NCSX design point was initially obtained by shaping a reversed shear advanced tokamak (ARIES design) three dimensionally. The 3D shaping generates external rotational transform while maintaining quasi-axisymmetry. As a result, the iota profile is monotonically increasing until near the edge of plasma (or reversed shear for most of the minor radius in tokamak sense). We will show that stability of external kink modes and the vertical mode can be improved over those of advanced tokamaks by external rotational transform and pure 3D geometric effects.

First we consider the effects of external rotational transform on kink and vertical stability. Compared to advanced tokamaks, QAS configurations have lower plasma current because the external rotational transform replaces part of current-generated transform in tokamaks (at fixed edge iota or q). As a result, the external kink and vertical mode stability is improved in QAS due to lower current. We find that find that the vertical mode (of n = 0 family) can be much more stable in QAS devices than in tokamaks [4]. The QAS configuration C82 is calculated to be robustly stable to the vertical mode at a high averaged elongation (κ ~ 2).

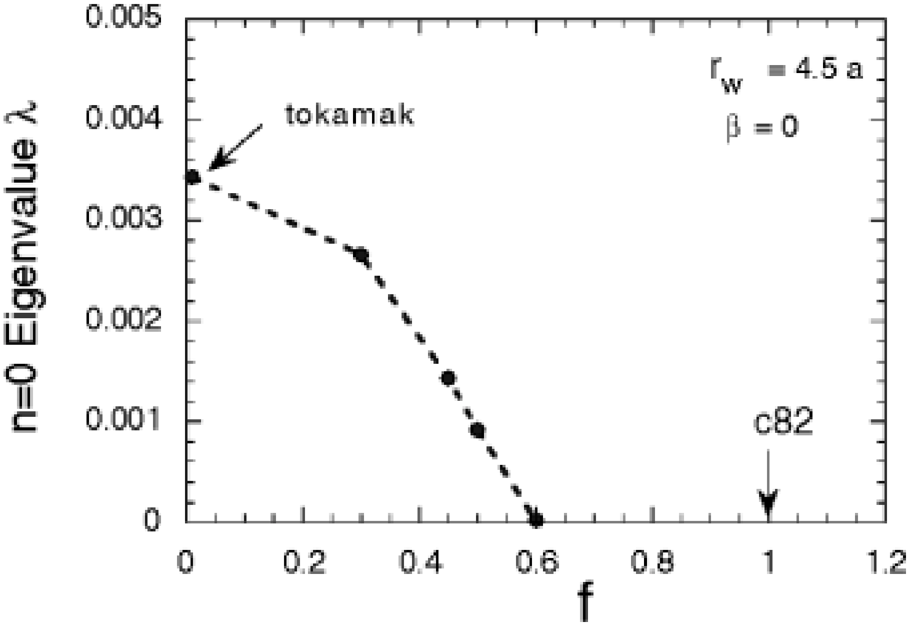

Figure 5-4. The eigenvalue of the vertical mode versus fraction of c82's nonaxisymmetric shape

Figure 5-4 shows the eigenvalue of the vertical mode as function of the fraction of nonaxisymmetric shape, f, at fixed current profile and zero beta. Here f = 1 corresponds to the full C82 shape and f = 0 corresponds a tokamak with the axisymmetric shape of C82. Equilibria are obtained by linear interpolation of the tokamak shape and the C82 shape (i.e., $R_{m,n}(f) = fR_{m,n}$, $Z_{m,n}(f) = fZ_{m,n}$ for $n \neq 0$, where $R_{m,n}$ and $Z_{m,n}$ are Fourier coefficients of the C82 shape). We observe that there is a large stability margin for the vertical mode in C82 with the marginal point at f = 0.6. The results of Fig. 5-4 are obtained with zero beta because of equilibrium convergence problem due to low ι at small f. At finite f, the effects of beta are found to be stabilizing. Thus, an even larger margin is expected at finite beta. This robust vertical stability is mainly due to effects of the external rotational transform. We have derived an analytic stability criterion for vertical mode in a large aspect ratio QAS with constant current density and constant external rotational transform [3]. The external rotational transform needed for stability is given by:

$$F_i = \frac{\kappa^2 - \kappa}{\kappa^2 + 1} \qquad (5\text{-}8)$$

where $F_i = \iota_{ext} / \iota_{total}$ is the fraction of external rotational transform and κ is the axisymmetric elongation. This criterion has been confirmed by the Terpsichore code, as shown in Figure 5-5. The calculated critical external transform (solid dots) agrees reasonably well with the analytic result (solid line). Physically, the external transform is stabilizing because the external poloidal flux enhances the field line bending energy relative to the current-driven term for the vertical instability. We note that $F_i = 0.5$, κ = 1.9 for C82 and Fi = 0.75 and κ = 1.8 for NCSX. Thus, both C82 and NCSX are very stable to the vertical mode according to this analytic criterion.

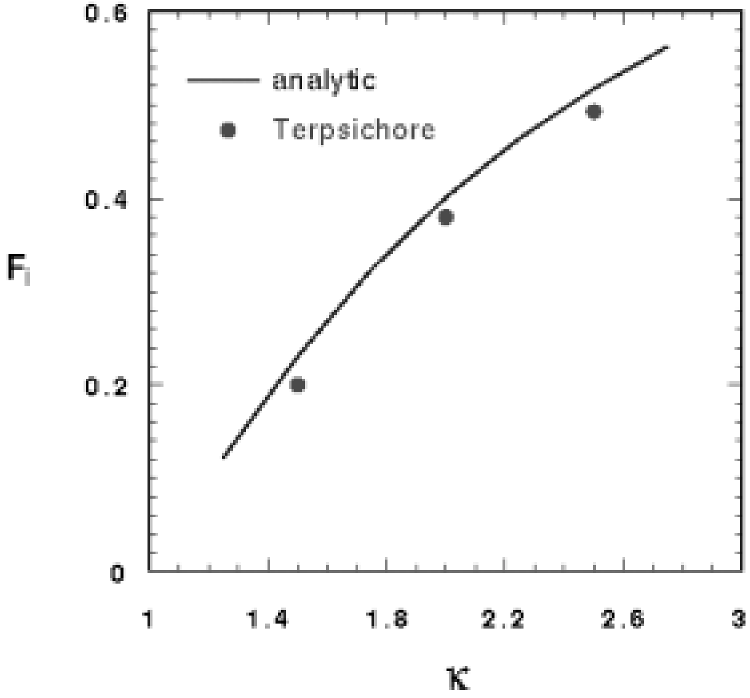

Figure 5-5. The critical value of fraction of external transform as function of axisymmetric elongation

Second, we show that external kink stability can be enhanced in QAS by controlling the iota profile via 3D shaping. Specifically, it is found that the edge magnetic shear is stabilizing for external kink modes [4]. Figure 5-6 shows the calculated N=1 external kink mode eigenvalue $\lambda = -\omega^2$ as a function of global magnetic shear near the edge defined by $\iota(1) - \iota(0.75)$ at $\iota(1) = 0.46$. These results are obtained for a $N_p = 4$ QAS with R/a = 2.1 and $\beta \sim 6.3\%$. The variation of shear is controlled entirely by 3D plasma boundary shape while keeping the current and pressure profiles fixed. We observe that the external kink mode is stabilized by edge magnetic shear. Physically, the shear is stabilizing because it enhances the field line bending energy.

Third, we show that external kink stability can also be enhanced in QAS by pure 3D geometry effects at fixed iota profile [4]. 3D shaping can affect important magnetic field properties in such a way so the MHD stability is favorable. In practice, favorable 3D shaping can be found by using a numerical optimizer that uses kink stability as a target function. Two examples are shown here to illustrate the pure geometry effects on MHD stability. The first example is an external kink stabilized by local magnetic shear controlled by 3D shaping. Figure 5-7 shows plasma cross-sections of a three field period R/a = 3.5 QAS before (left) and after (right) the stability optimization. The corresponding rotational transform profiles are shown in Figure 5-8.

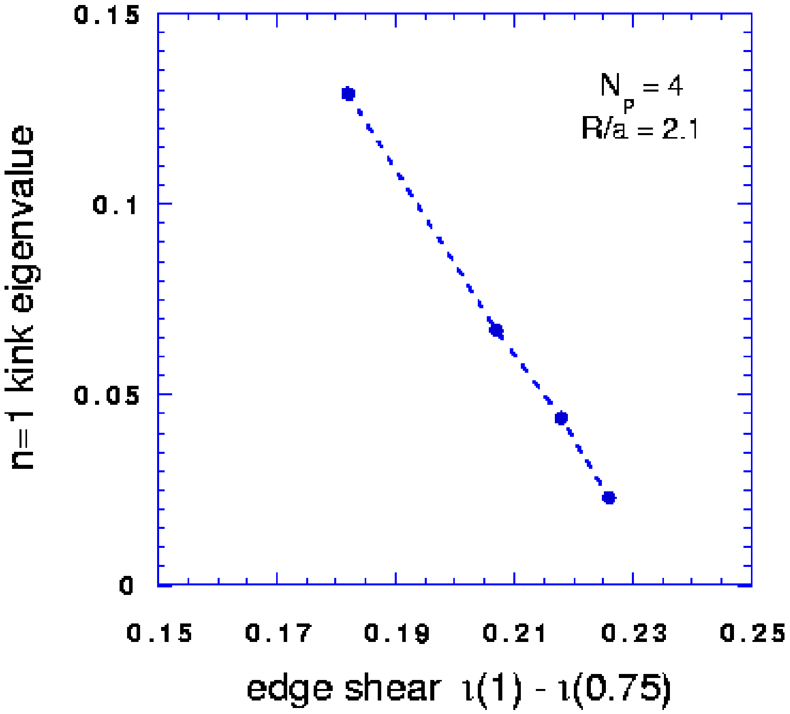

Figure 5-6. The n = 1 external kink eigenvalue versus edge magnetic shear for a four field period QAS with R/a = 2.1 and $\beta \sim 6.3\%$

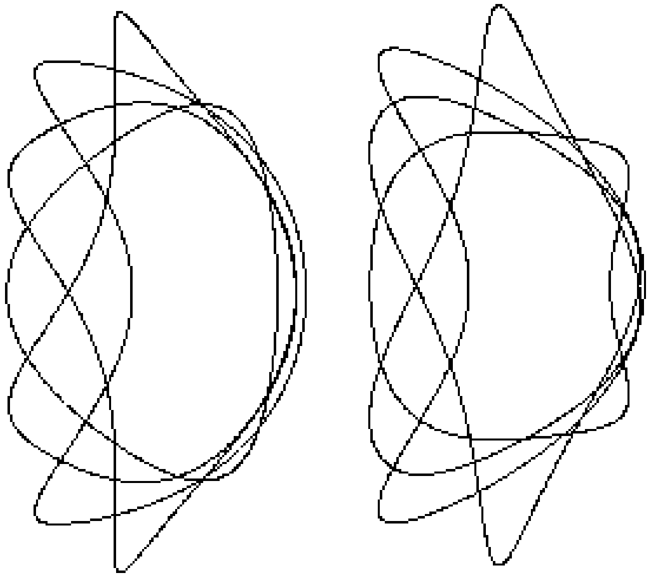

Figure 5-7. Plasma cross-sections of a three field period QAS before optimization (left) and after optimization (right)

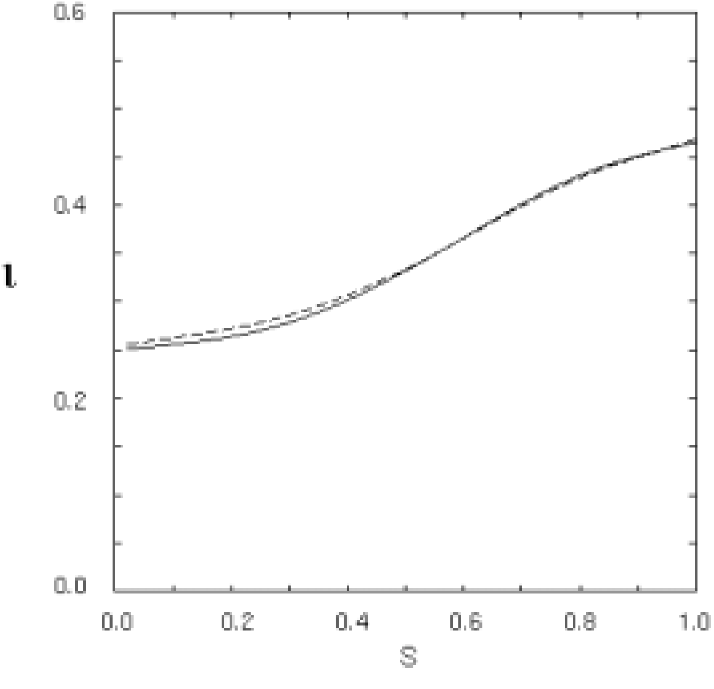

Figure 5-8. Iota profiles of a three field period QAS before optimization (solid line) and after optimization (dashed line)

The initial configuration (C3m) is unstable to an n = 1 kink with eigenvalue of $\lambda = 1.8 \cdot 10^{-3}$. Figure 5-9 plots the perturbed pressure contour of the corresponding eigenmode at the two symmetric cross-section (at $\phi = 0$ and $\phi = \pi/3$). The unstable mode peaks on the outboard side of the plasma (i.e., ballooning) due to destabilizing bad curvature. The final configuration after optimization (called C82) is marginally unstable with an eigenvalue of $\lambda = 2.6\times10^{-5}$ at $\beta = 3.9\%$. We note that the change in the iota profile from C3m's to C82's is minimal and the two order of magnitude reduction in kink eigenvalue can only be attributed to pure geometry effects due to 3D shaping. The major change in shaping from C3m to C82 is an indentation of plasma boundary on the outboard side at the half-period cross section that is found to be most effective for stabilization. To understand the 3D shaping effects on stability, we have evaluated changes in stabilizing and destabilizing terms from C3m's to C82's. Table 5-1 list the relative contributions of these terms normalized by the vacuum magnetic energy for both C3m and C82.

Table 5-1. The breakdown of stabilizing and destabilizing terms in the plasma potential energy normalized by the vacuum energy for the most unstable n = 1 external kink mode in C3m and C82

	Vacuum	line bending	kink	ballooning
c3m	1.00	4.05	-3.98	-1.72
c82	1.00	4.51	-3.87	-1.64

The line bending column in Table 5-1 corresponds to the sum of first and second terms in δW_p [Eq. (5-4)], while the kink and ballooning columns correspond to the third and the forth term respectively. We note that the parallel current term (kink column) contributes about 70% of the total destabilizing sum for both cases and is thus the main destabilizing mechanism for the n = 1 external kink modes, in accordance with usual expectation. However, the ballooning term also contributes significantly to the instability. This is the reason the mode exhibits the strong ballooning feature shown in Figure 5-9. Thus, the unstable mode should be called kink-ballooning mode. The pressure also contributes indirectly to the kink term through the parallel Pfirsch-Schluter current. For both cases, the Pfirsch-Schluter current contributes about 57% of the kink term. Thus, the pressure-induced Pfirsch-Schluter current is actually more important than the volume-averaged parallel current for these two configurations. We now discuss why the 3D shaping change from C3m to C82 stabilizes the external kink mode. We observe from Table 5-1 that the main difference between C3m and C82 is the field line bending term. This suggests that the effects of shaping on local magnetic shear play a significant role. Figure 5-10 shows the contours of local magnetic shear $\hat{S}$ of C82 on the s = 0.63 flux surface (the δW_p peaks approximately at this surface). Here, the local magnetic shear $\hat{S}$ is defined by $\hat{S} = -(\sqrt{g}/\Psi'^2)\, \mathbf{h} \cdot \nabla\times\mathbf{h}$ with $\sqrt{g}$ being the Jacobian and $\mathbf{h} = \mathbf{B} \times \nabla s / |\nabla s|^2$. Note that the global magnetic shear dq/ds is a surface average of $\hat{S}$ where $q = 1/\iota$. The value of local magnetic shear in Figure 5-10 ranges from -74.3 to 28.6, while the global shear is dq/ds = -2.4. This shows that the local magnetic shear is dominated by helical contribution and is much larger than the global shear. Figure 5-11 compares the local magnetic shear of C3m with that of C82 on the outboard side at s = 0.63.

Indeed we find that the local shear of C82 is substantially larger than that of C3m on the outboard side. This indicates that the local shear is responsible for the change in the field line bending energy and the stability between these two configurations.

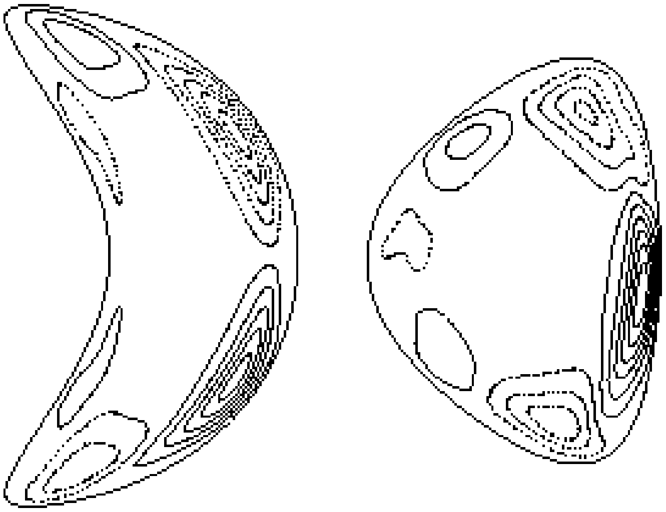

Figure 5-9. contours of perturbed pressure at the two symmetric cross-sections for C3m

.

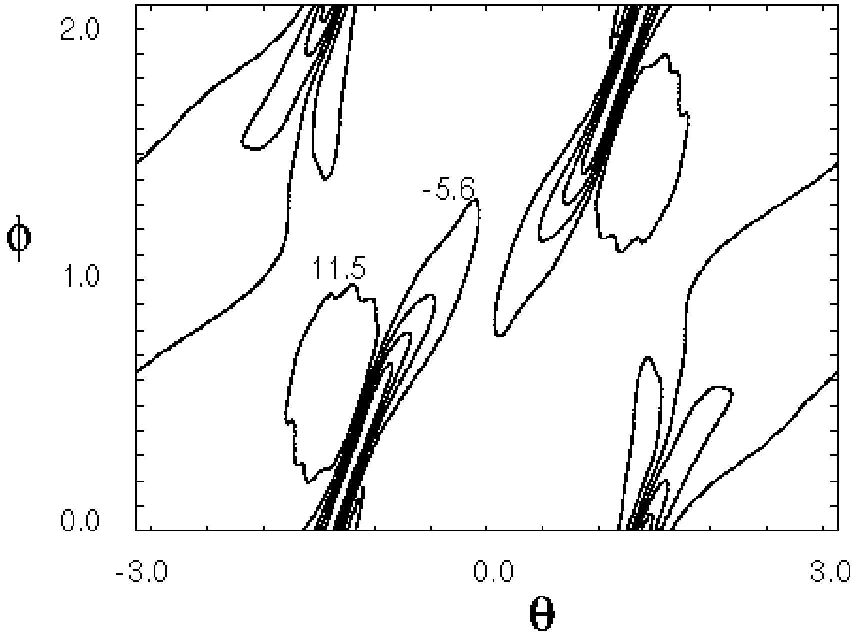

Figure 5-10. The contour plot of the local magnetic shear of the configuration c82 on the s = 0.63 flux surface for one field period ($0 < \phi < 2\pi/3$). The local shear value for some contours is marked

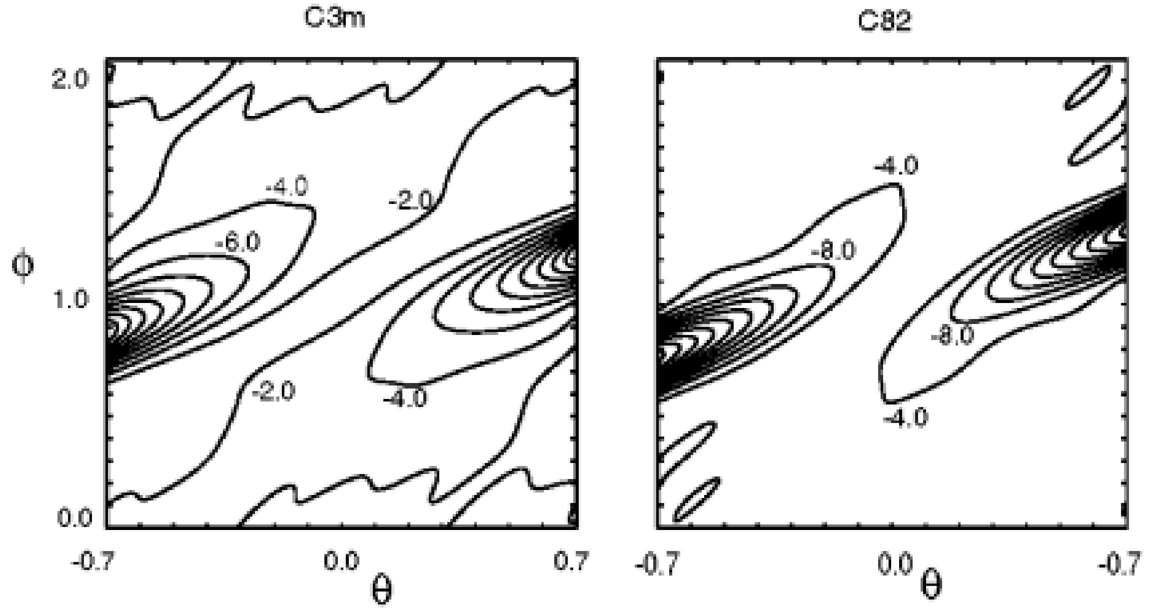

Figure 5-11. The contour plot of the local magnetic shear for the configuration C3m (left) and C82 (right) on the s = 0.63 flux surface on the outboard side of the torus (-0.7 < θ < 0.7). The local shear value for some contours is marked

We now discuss effects of magnetic well, which is a function of the 3D geometry. In our search for more robust configurations with good coil characteristics, we observed the importance of externally generated magnetic well on global MHD instability, especially the external kinks. Specifically we showed that the external kink stability is strongly correlated with the size of magnetic well. To isolate the effects of magnetic well, we generated a series of four QAS configurations with different magnetic wells. The shapes of last closed flux surfaces for each of the four configurations (labled KG7a, KG7b, KG7c and KG7d) are shown in Figure 5-12. The corresponding external magnetic well profiles, defined as $(1-V'(s)/V'(0))$ in the absence of the plasma current and pressure, are plotted in Figure 5-13. This series is generated by varying only a single term in the boundary harmonics, i.e., $Z(m,n) = Z(2,1)$., at fixed current and pressure profiles. By modifying this single term, we are able to change the magnetic well from a depth of 7% to 4%, 0%, and then -10% while maintaining approximately the same external iota profile (from 0.12 at center to 0.33 at the edge). The results of the N = 1 external kink stability from Terpsichore are shown in Figure 5-14 which plots the kink eigenvalue as function of plasma beta for each of the configurations. We observe that the beta limit increases from 2.2% (KG7e) to 5.2% (KG7a) as the corresponding magnetic well varies from -10% (magnetic hill !) to 7%. The calculations for the N = 0 family showed that the critical beta is always higher than those for the N = 1 instability. Since the rotational transform profiles of these cases are similar for these configurations, the difference in the kink stability can be attributable to the difference in the magnetic well. Physically, a strong magnetic well reduces the pressure gradient drive (ballooning term) and enhances the stability of global kink modes.

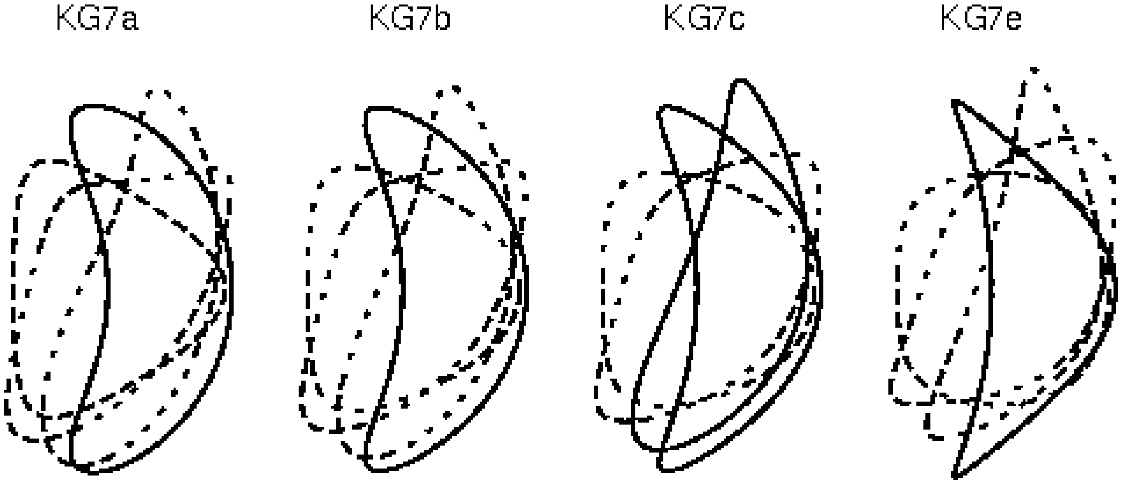

Figure 5-12. Poincare sections equally spaced over half a field period for four configurations with decreasing depths of externally generated magnetic well

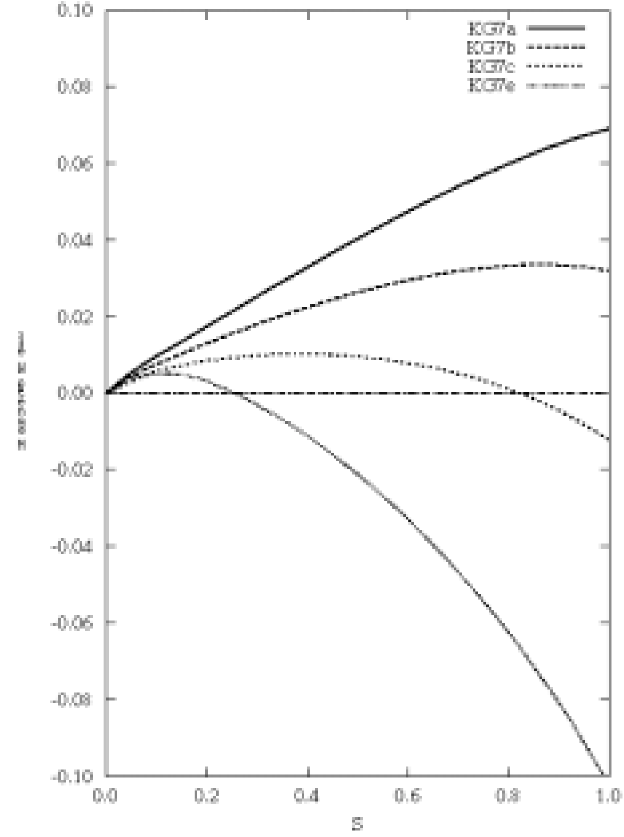

Figure 5-13. Vacuum magnetic well as a function of s

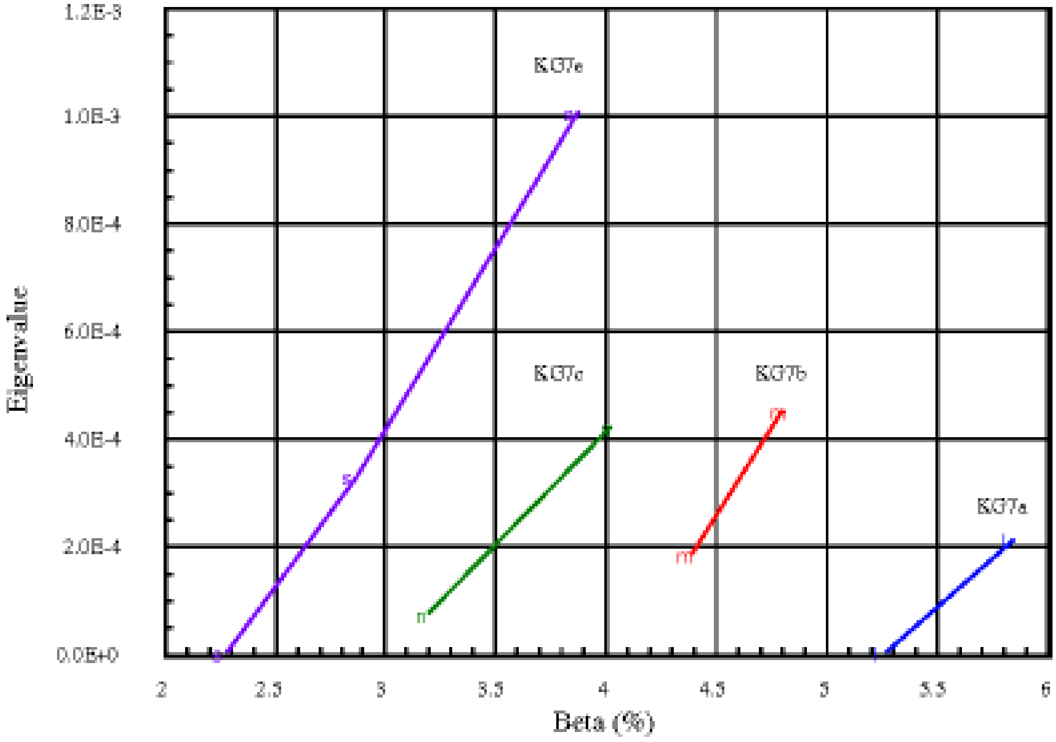

Figure 5-14. Eigenvalue of the N = 1 external kink mode versus averaged plasma beta for four configurations with increasing depths of magnetic well

5.4 Stability of NCSX configuration

Here we will present stability results for the NCSX reference configuration (LI383) in terms of Mercier stability, ballooning stability and, external kink and vertical mode stability. The NCSX configuration was found by optimizing the MHD stability of Mercier, ballooning and external kink modes along with quasi-symmetry and other desired targets. Thus, the configuration is designed to be stable (marginally) to all these modes. However, absolute stability is not guaranteed for several reasons. First, the stability evaluations in the optimizer are not complete. For example, the N = 0 family of modes were not included in the original optimization, but were checked afterwards. Similarly for ballooning stability, only two field lines are calculated at each flux surface. Second, the numerical resolutions used are fairly crude for the sake of speed and available memory. Here, we show a more complete stability analysis and convergence study to validate the optimization results.

5.4.1 Mercier Stability

Figure 5-15 shows the Mercier criterion (> 0 for stability) as a function of the normalized toroidal flux s. It is evident that Mercier modes are stable over the whole radii of the plasma. As stated in the preceding sections, the NCSX configuration was designed to have magnetic well in vacuum. The magnetic well is maintained in the full beta full current reference configuration. Thus, the favorable Mercier stability is not surprising.

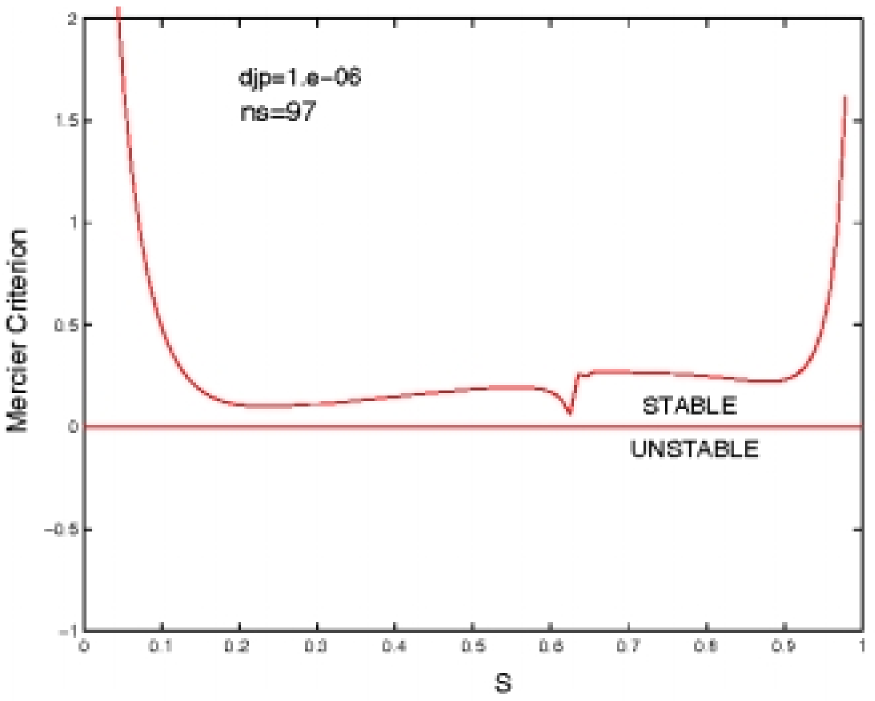

Figure 5-15. Mercier criterion for the NCSX reference configuration

5.4.2 Ballooning Stability

Figure 5-16 plots the ballooning eigenvalue (> 0 for instability) versus S calculated with the Terpsichore-VVBAL (solid line) and COBRA (solid star). We note that two codes give same marginal points (The absolute values of the eigenvalue differ because different definitions of the eigenvalue are used in the two codes). The results are obtained using parameters of $\theta_k = 0$ and $\alpha = \pi/3$ for which the ballooning modes are determined to be most unstable. The results are converged in terms of number of radial grid points and the number of Boozer modes for the equilibrium mapping. Figure 5-17 shows that the Terpsichore-VVBAL ballooning eigenvalue does not change when the number of Boozer modes is increased from 715 to 853. These results show that the NCSX configuration is ballooning stable over most of the plasma radii except in a small region near the edge. This weak ballooning instability can easily be re-stabilized by a slight change in the 3D boundary shape or by local flattening of the plasma gradient. Therefore, the NCSX configuration can basically be regarded as ballooning stable.

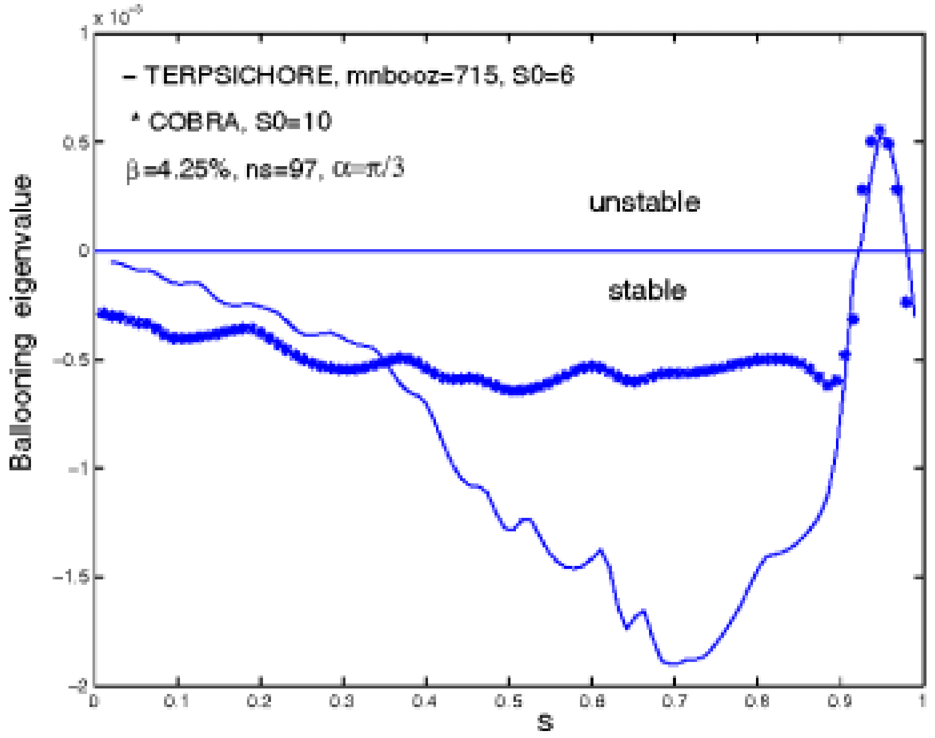

Figure 5-16. Ballooning eigenvalue as a function of S for the NCSX reference configuration

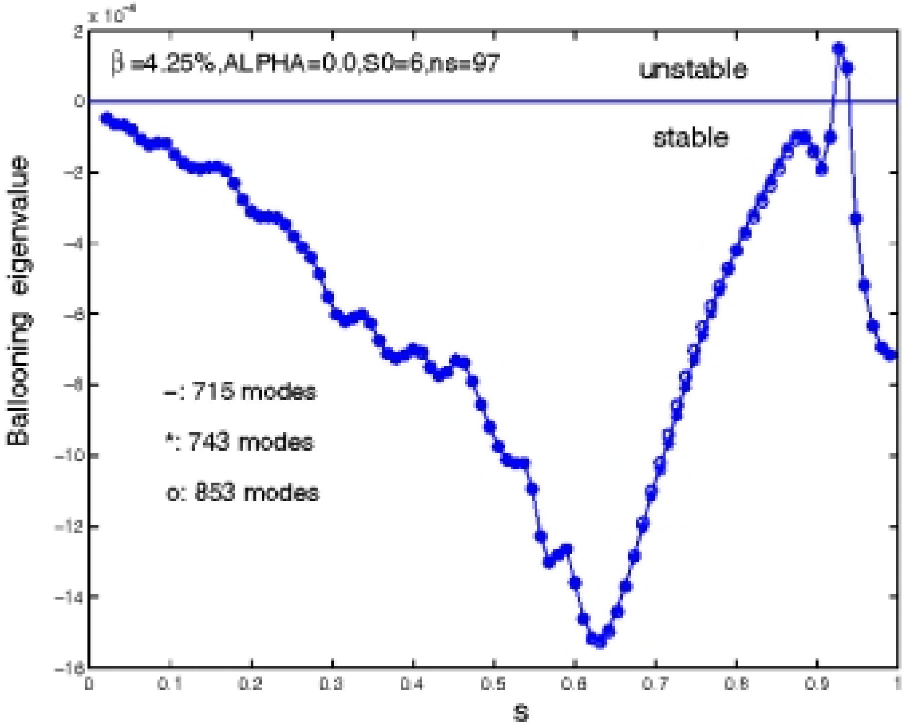

Figure 5-17. ***Ballooning eigenvalue as a function of S for the NCSX reference configuration***

The stability results presented here are valid for infinite-n ideal modes. In practice, only finite-n modes can be unstable due to Finite Ion Larmor Radius (FLR) stabilization. Thus, an important issue is the stability of finite n ballooning modes and associated beta limits. We had carried out finite-n ballooning mode stability calculations using the global code Terpsichore for the configuration C82. The results showed that the finite n ballooning modes (n ~ 20) are significantly more stable than the Infinite-n results [6]. Work is in progress [21] to study the FLR stabilization of finite n ballooning modes by applying the WKB ballooning formalism and the quantum chaos theory [22].

5.4.3 External Kink and Vertical Stability

As mentioned before, the NCSX configuration was optimized to be marginally stable to the N = 1 family of external kink modes using a low resolution. Typically 49 radial grid points, 94 VMEC modes, 264 Boozer modes for mapping, and 91 modes (n 7) for perturbation are used with Terpsichore in the optimization. Here we show a more complete stability analysis for both the N = 1 and the N = 0 families using higher resolutions.

We have carried out a systematic convergence study for the stability of global MHD modes in the NCSX configuration using Terpsichore. Up to 300 radial grid points, 218 VMEC modes, 414 Boozer mapping modes, and 361 modes (n 26) for perturbation are used. We found that the stability is most sensitive to number of perturbation modes. Since the NCSX configuration is optimized to be marginal to the external kinks, we use two artificial multipliers, coec and coep for the kink and ballooning terms in δW respectively, to adjust the size of the two destabilizing terms. In this way, we can determine how far an equilibrium is from marginal stability boundary by varying these two coefficients.

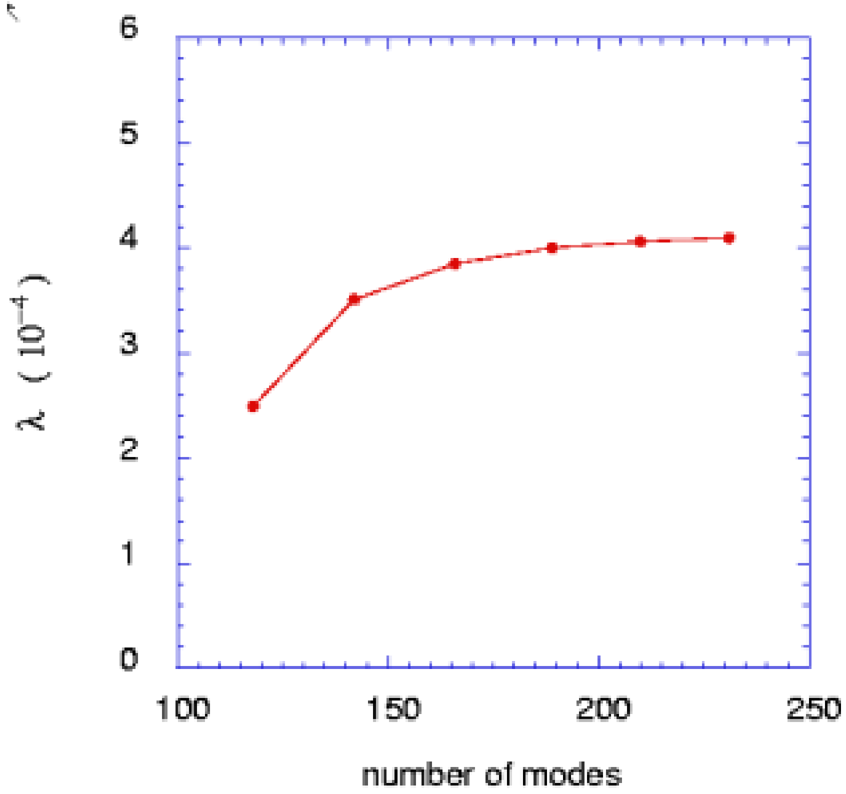

Figure 5-18. The N = 1 kink eigenvalue as function number of perturbation Fourier modes for the NCSX reference configuration.

Figure 5-18 shows the N = 1 kink eigenvalue λ as a function of number of the perturbation modes (at coep = coec = 1.025) for the mode with (m,n) = (17,11) being the largest harmonic. We observe that the eigenvalue converges for > 190 modes. Figure 5-19 shows the kink eigenvalues as function of coep (coec = coep) for the three most unstable modes of the N = 1 family. Note that in general there are many eigenmodes for the same mode family with different harmonic distribution. In Figure 5-19, the largest harmonic for each of the three eigenmodes are (17,11) (solid diamonds), (2,1) (solid dots), and (8,5) (solid square) respectively. The corresponding normal component of plasma displacement vector (versus radius) is shown in the Figure 5-20 on the left for the most unstable eigenmode. We observe that the eigenmode with the dominant (17,11) is the most unstable and yields a critical value of coep = coec = 0.925. This shows that, at β = 4.25%, the NCSX configuration (fixed boundary VMEC equilibrium) is weakly unstable to the N = 1 external kink with a small growth rate on order of 10^{-4}. This weak instability can be easily stabilized by modifying the 3D shape slightly as shown at the end of this subsection.

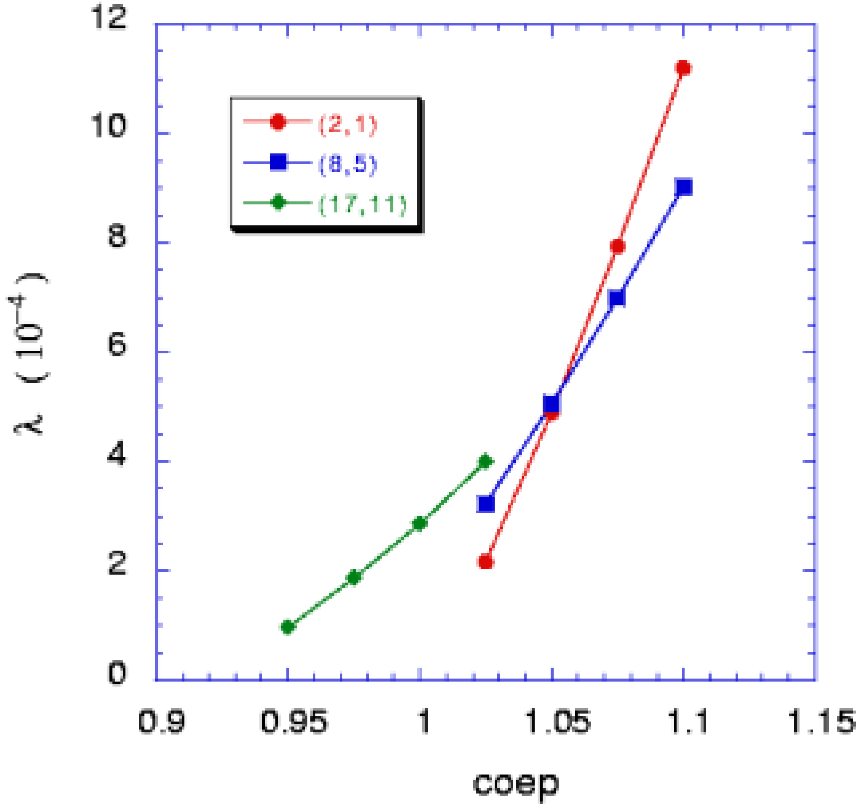

Figure 5-19. ***The N = 1 eigenvalues versus coep for the three most unstable modes***

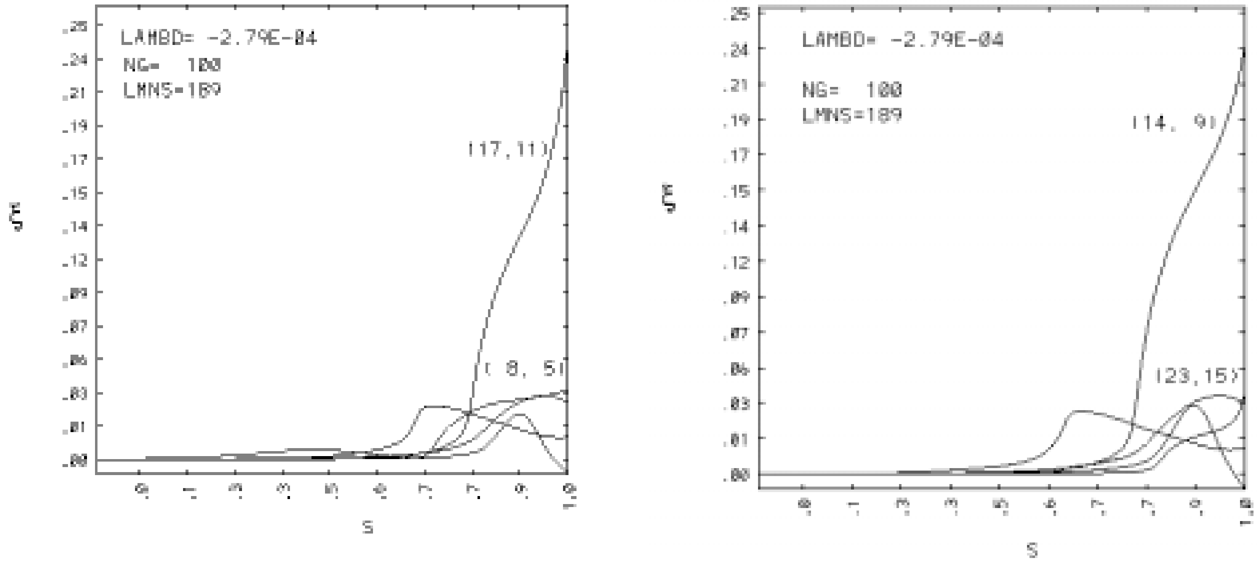

Figure 5-20. The radial displacement of the N = 1 (left) and N = 0 (right) most unstable eigenmode at coep = coec = 1.0 .

We now show results for the N = 0 family of modes, including the vertical mode for which the (1,0) harmonic is dominant. Figure 5-21 on the left shows the most unstable eigenvalue of the N = 0 family versus coep = coec with (m,n) = (14,9) being the dominant harmonic. The corresponding eigenfunction is shown in Figure 5-20 on the right. We observe that this mode yields a similar critical coep as compared to the N = 1 family. The stability of the vertical mode with dominant (1,0) is shown in Figure 5-21 on the right. The results are obtained at fixed coep = 1 and only the flux-averaged part of the parallel current in the kink term is being changed by coec. The corresponding eigenfunction at coec = 2.2 is shown in Figure 5- 22. The (1,0) harmonic is clearly dominating, as it should be for a vertical mode. We observe that the vertical mode would become unstable if the plasma current were raised by a factor of two. Thus, the NCSX configuration is robustly stable. This is expected from our simple analytic results due to a large external rotational transform.

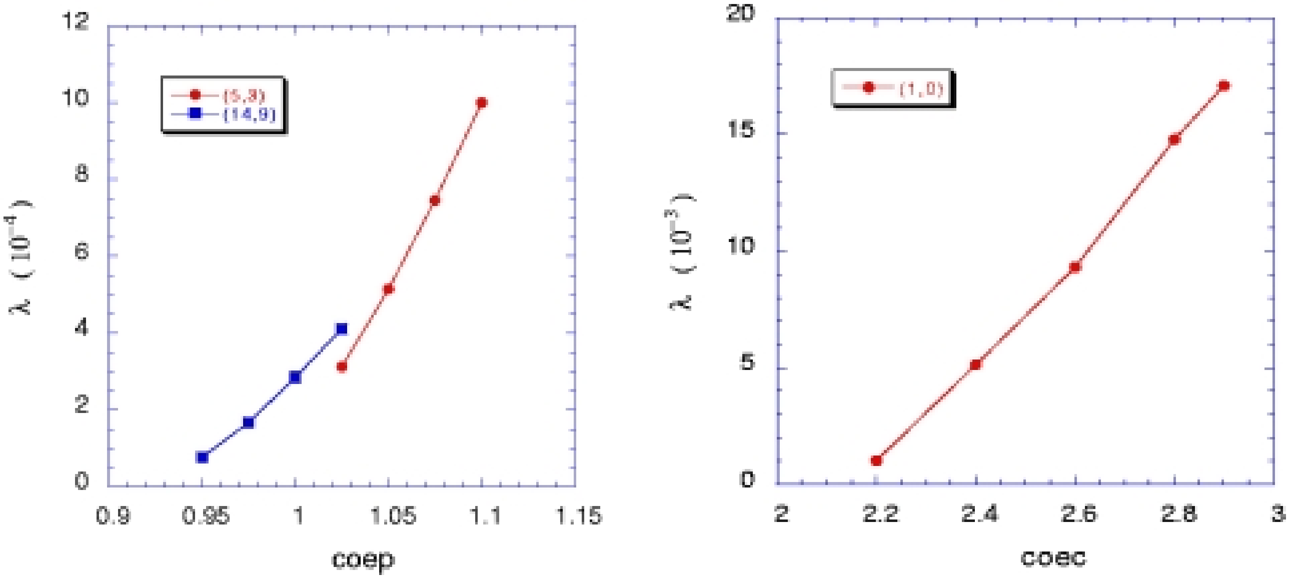

Figure 5-21. The N = 0 eigenvalue versus coep for the most unstable mode (left) and the vertical mode (right)

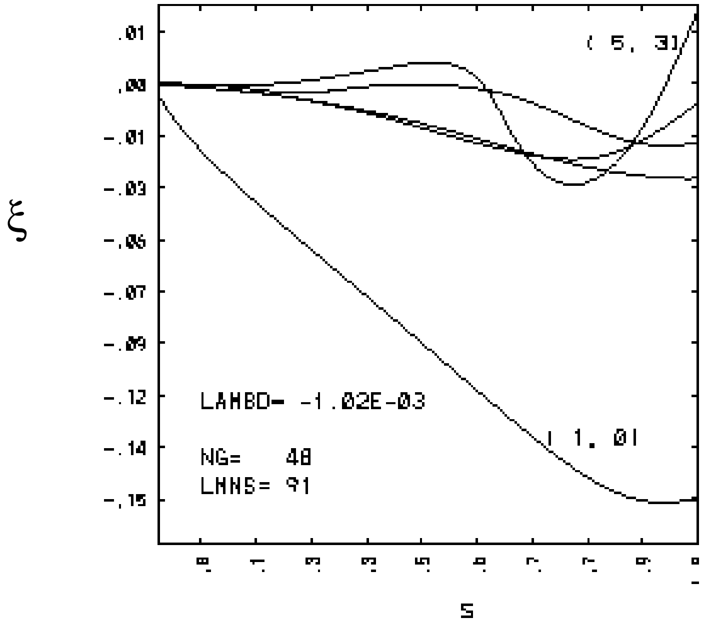

Figure 5-22. ***The radial displacement versus radius for the vertical mode.***

Finally, we demonstrate here that the weak high-n kink instabilities of the NCSX configuration (LI383) can be easily re-stabilized with a small change in the boundary shape. Figure 5-23 shows the cross-sections of the original LI383 (black) and the modified configuration LI383_B (red) that has been re-optimized for kink stability. The new configuration is calculated to be robustly stable to both N=1 and N=0 families of external kink modes with up to 201 perturbation modes (toroidal mode number up to 20). We observe that the shape change from LI383 to LI383_B is minimal.

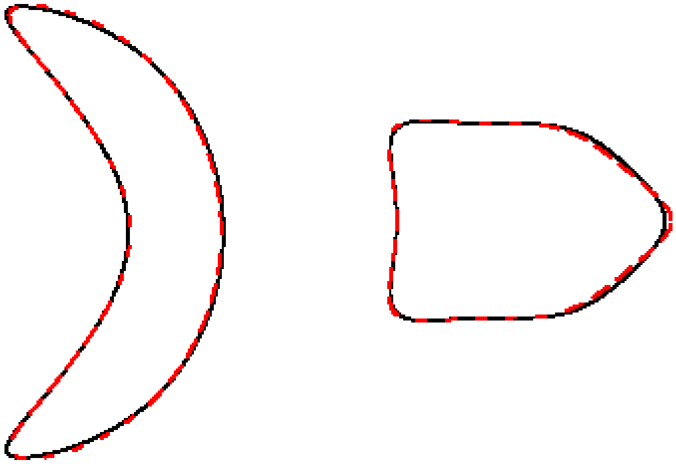

Figure 5-23.The comparison of cross-sections of the original LI383 configuration (black solid line) and the modified LI383 configuration (red dashed line) which is re-optimized to be stable to external kink modes

5.5 Effects of Wall on Kink Stability

In the preceding section, the wall is prescribed to be more than twice the minor radius away from the plasma edge so that the effects of wall on the kink stability is negligible. Here we investigate whether a much closer wall (say $d_{wall} \sim 0.3 < a >$) could have a significant effect on the beta limit. This is motivated by the fact that in an actual experiment, the vacuum vessel is close to the plasma over a significant fraction of the surface and they could influence the stability of external kink modes.

Figure 5-24 shows the most unstable eigenvalue of the N = 1 family as a function of the wall distance from the plasma edge, d_{wall} for the LI383 configuration. The plasma beta is raised from the baseline $\beta = 4.25\%$ to $\beta = 5.0\%$ with fixed plasma boundary shape in order to have instability with a close wall. The solid dots correspond to a fixed baseline plasma current whereas the solid square correspond to an enhanced plasma current proportional to the plasma beta. A conformal conducting wall is prescribed for these results. We observe that for both cases, stabilization of the external kinks (at $\beta = 5\%$) requires a very close fitting wall at about $d_{wall} \sim 0.05$ or $d_{wall}/ < a > \sim 0.1$. This means that both the vacuum vessel and the conducting structures are not expected to affect the kink stability significantly in a real discharge of NCSX.

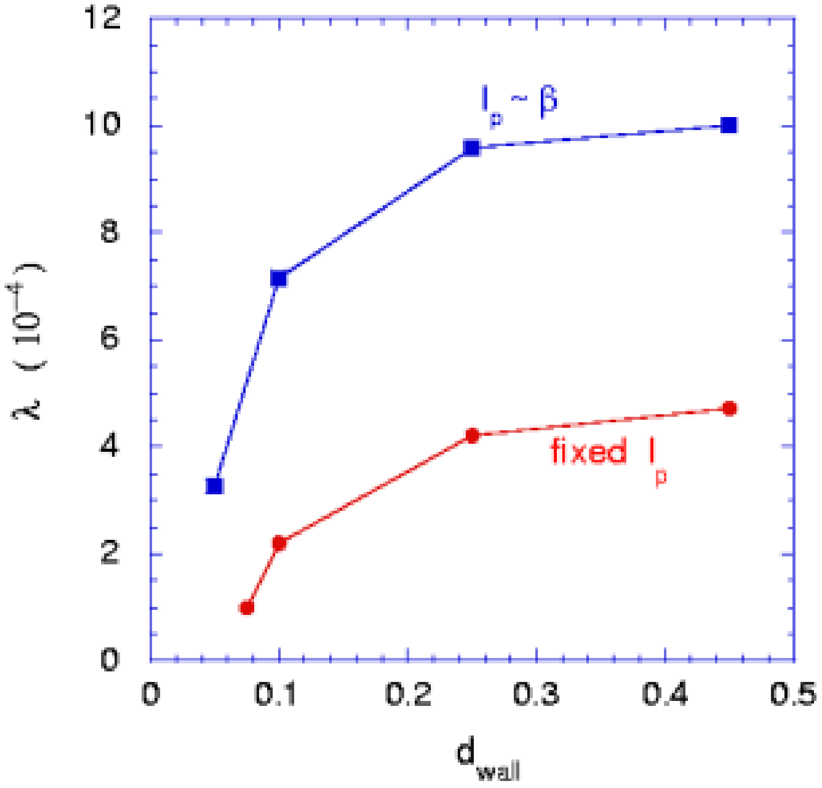

Figure 5-24. The N = 1 eigenvalue as function of wall distance for the NCSX configuration at $\beta = 5\%$

5.6 Alfvén Mode Stability

It is known that energetic particles can resonantly destabilize shear Alfvén waves, such as Toroidal Alfvén Eigenmode (TAE), by tapping the free energy associated with their pressure gradient. TAEs are stable discrete shear Alfvén modes formed as a result of mode coupling of neighboring poloidal modes. Because TAEs are weakly damped, they are most susceptible to energetic particle destabilization. Since their discovery in 1985, TAEs have been routinely observed in NBI-heated tokamak plasmas (TFTR, DIIID, JT-60U) driven by fast neutral beam ions and in ICRH-heated plasmas driven by fast minority ions (TFTR, JT-60U, JET) [23]. Alpha particle-driven TAEs were first observed in the TFTR DT experiments [24]. NBI-driven TAEs have also been observed in stellarators (W7-AS [25], CHS and LHD [26]). TAE instability can sometime cause large losses of energetic ions, resulting in low heating efficiency.

In NCSX, the plasma is heated by neutral beam heating. Thus, questions naturally arise: can TAEs be destabilized in NCSX? If so, is there significant beam ion loss due to the instability?

A necessary condition for TAE instability is to satisfy the wave particle resonances (either $v_{||} = v_A$ or the sideband $v_{||} = v_A/3$.). For the NCSX standard high-beta operation, the main parameters at $\beta = 4\%$ are: $B_0 = 1.2T$, $R_0 = 1.4m$, the central electron density $n_e(0) = 7.7\times10^{13}$ (cm^{-3}), and $\beta_{beam} \sim 0.5\%$. The neutral beam ions (hydrogen) are injected tangentially into hydrogen plasmas at 50kev. Thus, we have $v_{||} /v_A \sim 1.0$ and the resonance condition can easily be met.

The TAE stability in NCSX, on the other hand, is subtler. To excite TAEs, the beam ion drive must exceed the mode damping. However, both the drive and the damping are sensitive function of plasma parameters and profiles. Furthermore, the 3D geometry of NCSX introduces another variable in this equation. Thus, there is no reliable ways to predict the TAE stability threshold without a systematic numerical modeling.

In actual tokamak experiments, the critical beam ion beta for instability varies widely, from $\beta_{beam,crit} \sim 0.1\%$ in the NNBI-heated JT-60U plasmas to $\beta_{beam,crti} \sim 0.5\%$ in the NBI-heated DIIID plasmas. Since $\beta_{beam} \sim 0.5\%$ at 5MW of beam heating power in NCSX, the TAE instability is possible in this device.

Although we expect the physics of TAE stability and related transport in QAS to be similar to that in tokamaks, the 3D geometry of NCSX does introduce important new physics effects. Because the mode coupling and Alfvén spectrum depend not only on the magnetic field strength but also on 3D geometry, significant mode coupling between different toroidal mode numbers is expected especially for high-n modes. This would result in additional continuum damping. This new mode coupling would also produce new types of Alfvén eigenmodes with their frequencies typically higher than TAE's. Another important difference is in q profiles (or iota profiles). Unlike in tokamaks, the NCSX has a q profile monotonically decreasing in radius until the very edge of the plasma. Thus, the Alfvén continuum gaps are not aligned over the whole plasma. This implies that the continuum damping is expected to be significant for global

TAEs and the TAE instability is most likely to be located near the center of plasma, as observed in LHD [26].

In NCSX, the linear stability and nonlinear dynamics of TAE or other type of Alfvén Eigenmodes can be studied systematically over wide range of parameter space. In particular, the new physics introduced by the 3D geometry can be studied by varying the 3D shaping via coil currents. In this regard, we anticipate adding a set of coils to excite Alfvén eigenmodes externally, as has been done in JET using its saddle coil system [27]. This capability will allow measurement of Alfvén eigenmode frequencies and their damping rates and thus a systematic study of 3D effects on TAE stability.

5.7 Summary

We have presented the physics basis for ideal MHD stability in NCSX. The highlights of this chapter are as follows.

The most advanced MHD stability codes were used in the design of NCSX. We have validated these modern codes by benchmarking two independent local stability codes for infinite-n ballooning modes (Terpsichore-VVBAL and Cobra) and two independent global MHD stability codes for external kink modes (Terpsichore and CAS3D).

We have identified four physical mechanisms for stabilization of external kink modes and the vertical mode via 3D shaping. It was shown that 3D shaping can stabilize the vertical mode via external rotational transform and that 3D shaping can stabilize the external kink modes via magnetic shear (both global and local) and vacuum magnetic well.

Extensive convergence study has been done for both ballooning modes and external kink stability in the NCSX reference configuration (fixed boundary LI383 at β = 4.25%), which was optimized to be marginally stable. A weak high-n external kink instability was found at higher numerical resolutions and was re-stabilization by a small change in the 3D shape.

References

[1] G. Y. Fu, L. P. Ku, N. Pomphrey *et al.*, in the 17th IAEA Fusion Energy Conference, Yokohama, Japan, 19-24 October 1998 (International Atomic Energy Agency, Vienna) paper THP1/07.

[2] A. Reiman, G. Fu, S. Hirshman *et al.*,Plas. Physics and Contr. Fusion **41** (1999) B273.

[3] G. Y. Fu, Phys. Plasmas **7** (2000) 1079.

[4] G. Y. Fu, L. P. Ku, W. A. Cooper *et al.*, Phys. Plasmas **7** (2000) 1809.

[5] M. H. Redi, A. Diallo, W. A. Cooper *et al.*, Phys. Plasmas **7** (2000) 2508.

[6] G. Y. Fu *et al.*, the 18th IAEA Fusion Energy Conference, Sorrento, Italy, 4-10 October 2000 (IAEA, Vienna) paper TH3/2.

[7] W. A. Cooper et al., Nucl. Fusion **29** (1989) 617.

[8] R.Sanchez, S.P.Hirshman, J.C.Whitson and A.S.Ware, JCP **161** (2000) 589.

[9] R. Sanchez et al., CPC, 2001.

[10] D. V. Anderson, W. A. Cooper, R. Gruber, S. Merazzi, and 115 U. Schwenn, Scient. Comp. Supercomputer II, 159 (1990).

[11] C. Nuehrenberg, Phys. Plas. **3** (1996) 2401.

[12] S. P. Hirshman and J. C. Whitson, Phys. Fluids **26** (1983) 3553.

[13] ref for Boozer coordinates.

[14] I. B. Bernstein, E. A. Frieman, M. D. Kruskal and R. M. Kulsrud, Phys. Fluids, Proc. R. Soc. London Ser. A **244** (1958) 17.

[15] G. Y. Fu, W. A. Cooper, R. Gruber, U. Schwenn, D. V. Anderson, Phys. Fluids B**4** (1992) 1401.

[16] R. C. Grimm, J. M. Greene, J. L. Johnson, Methods Comput. Phys. **16** (1975) 273.

[17] S. C. Jardin, C. E. Kessel, C. G. Bathke et. al., Fusion Engr. and Design **38** (1997) 27.

[18] D. Dobrott and C. S. Chang, Nuclear Fusion **21** (1981) 1573.

[19] M. H. Redi, et al., EPS, Budapest, Hungary (2000).

[20] M. H. Redi, C. Nuehrenberg, W. A. Cooper, G. Y. Fu, C. Kessel, L. P. Ku, the 26th EPS Conference on Controlled Fusion and Plasma Physics, Maastricht, Netherlands, 1999 (The European Physical Society) Paper P4.085.

[21] M. H. Redi et al., "Ballooning Mode Instability of Compact Quasiaxially Symmetric Stellarators", in preparetion (2001).

[22] R. L. Dewar, P. Cuthbert, R. Ball, Phys. Rev. Lett. **86** (2001) 2321.

[23] K. L. Wong, Plasma Phys. Controlled Fusion **41** (1999) R1.

[24] R. Nazikian, G. Y. Fu, S. H. Batha et al, Phys. Rev. Lett. **78** (1997) 2976.

[25] A. Weller et al, in the 17th IAEA Fusion Energy Conference, Yokohama, Japan, 19-24 October 1998 (International Atomic Energy Agency, Vienna) paper EX2/1

[26] K. Toi, M. Takechi, M. Isobe et al, Nucl. Fusion **40** (2000) 1349.

[27] A. Fasoli, D. Borba, B. Breizman et al, Phys. Plasmas **7** (2000) 1816.